

Uncertainty Mitigation and Intent Inference: A Dual-Mode Human-Machine Joint Planning System

Zeyu Fang¹, Yuxin Lin³, Cheng Liu², Beomyeol Yu², Zeyuan Yang², Rongqian Chen¹,
Taeyoung Lee², Mahdi Imani³ and Tian Lan¹

Abstract—Effective human-robot collaboration in open-world environments requires joint planning under uncertain conditions. However, existing approaches often treat humans as passive supervisors, preventing autonomous agents from becoming human-like teammates that can actively model teammate behaviors, reason about knowledge gaps, query, and elicit responses through communication to resolve uncertainties. To address these limitations, we propose a unified human-robot joint planning system designed to tackle dual sources of uncertainty: task-relevant knowledge gaps and latent human intent. Our system operates in two complementary modes. First, an uncertainty-mitigation joint planning module enables two-way conversations to resolve semantic ambiguity and object uncertainty. It utilizes an LLM-assisted active elicitation mechanism and a hypothesis-augmented A^* search, subsequently computing an optimal querying policy via dynamic programming to minimize interaction and verification costs. Second, a real-time intent-aware collaboration module maintains a probabilistic belief over the human’s latent task intent via spatial and directional cues, enabling dynamic, coordination-aware task selection for agents without explicit communication. We validate the proposed system in both Gazebo simulations and real-world UAV deployments integrated with a Vision-Language Model (VLM)-based 3D semantic perception pipeline. Experimental results demonstrate that the system significantly cuts the interaction cost by 51.9% in uncertainty-mitigation planning and reduces the task execution time by 25.4% in intent-aware cooperation compared to the baselines.

I. INTRODUCTION

Human-robot collaboration has become a fundamental capability for autonomous systems in real-world missions such as healthcare, manufacturing, and disaster response [1], [2], [3]. AI agents are expected to function as human-like teammates that are capable of communication, understanding, and cooperation, instead of simply being tools that amplify human capabilities or generate human-like responses [4], [5]. In these scenarios, effective performance relies not only on the autonomy of the robot but also on its ability to reason and comply with human intentions and commands [6]. However,

open-world human-robot joint planning often faces significant challenges from uncertainties: task-relevant factors (e.g., object properties, instruction semantics, and human intent) are often ambiguous, obscure, or partially observable, creating knowledge gaps that can alter transitions, constraints, and goals within the deployed environment, and thus degrade planning quality if ignored or handled improperly [7], [8].

Categorized by the modality of human involvement, existing methods on human-robot collaboration can be broadly bifurcated into two approaches: explicit human-guided planning, where human input is restricted to high-level instructions, and implicit human intent inference, where the human directly participates in the task execution, and the robot infers human intent only from its observations without communication. [9], [10], [11]. For the human-guided approach, traditional methods to incorporate human feedback into planning, including Human-In-The-Loop (HITL) [12], [13], human-aware task planning [14], and interactive learning [15], largely treat humans as passive supervisors providing expert demonstrations or corrections, instead of facilitating task-relevant knowledge exchange through two-way communication [16], [17]. Recent work leverages large language models (LLMs) to translate natural-language instructions into executable robot actions [18], [19], extends static goal prediction to continual inference under evolving human preferences [20], and frames joint planning as a bidirectional, interactive process [21], [22]. However, many of these systems do not explicitly model uncertainty and may plan under unreliable assumptions. Moreover, they rarely maintain an explicit model of the knowledge gap during interaction, leading to redundant, lengthy questions and inefficient communication. In contrast, intent-inference methods such as Bayesian methods [23], [24], [25], Partially Observable Markov Decision Process (POMDP) models [26], [27], [28], and Cooperative Inverse Reinforcement Learning (CIRL) [26], [29], fail to actively reason about the intent evolution of humans over the long-horizon in order to predict future human intent. Recent LLM-based intent reasoning [30] offers greater expressiveness, yet its high computational cost and latency often limit deployment in real-time collaboration. There exists an important gap in creating autonomous agents that can actively model, reason, query, and elicit responses.

To address these limitations, we propose an end-to-end unified human-robot joint planning system that connects the perception model and low-level drone controller with a core planning engine, supporting two complementary planning

¹Zeyu Fang, Rongqian Chen, and Dr. Tian Lan are with Department of Electrical and Computer Engineering, George Washington University joey.fang@gwu.edu, rongqianc@gwu.edu, tlan@gwu.edu

²Cheng Liu, Beomyeol Yu, Zeyuan Yang and Dr. Taeyoung Lee are with the Department of Mechanical and Aerospace Engineering, George Washington University chengl@gwu.edu, yubeomyeol@gwu.edu, zeyuan.yang@gwu.edu, tylee@gwu.edu

³Yuxin Lin and Dr. Mahdi Imani are with the Department of Electrical and Computer Engineering, Northeastern University lin.yuxi@northeastern.edu, m.imani@northeastern.edu

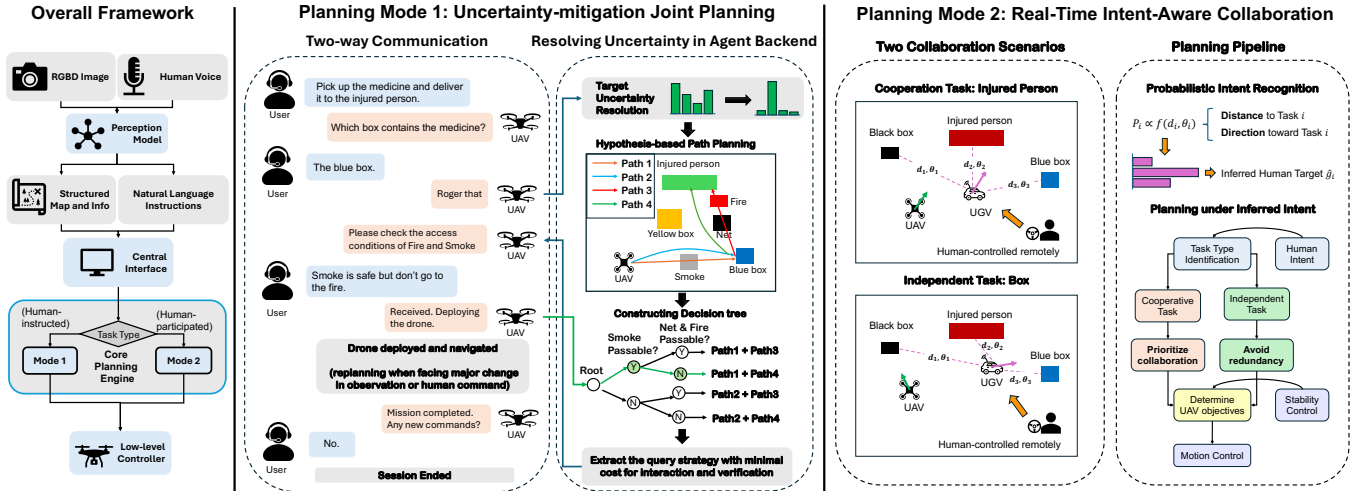


Fig. 1: Overview of the proposed system and the illustrations of the two modules inside the core planning engine supporting different planning modes. The system started with analyzing surrounding environments via perception models. Next, the central interface will activate one of the planning mode based on the task type to begin planning. The planning results will be present as either paths with way-points or high-level goals, and sent to the low-level controller, which will then drive the drone to carry out the plan. The details of the two planning mode are further elaborated in Section II.

modes: *uncertainty-mitigation joint planning* and *real-time intent-aware collaboration*, as shown in Figure 1. The system is mainly designed for search-and-rescue scenarios involving drones. It starts with information gathering from the surrounding environments via perception models. Next, a central interface is presented for human interactions. Depending on the task type, one of the planning modules will be activated from the core planning engine, which analyzes the information, resolves the uncertainties, and then drafts refined plans. These plans will finally be sent to the low-level controller for drone deployment.

Within the first planning mode, the robot receives a natural-language task instruction; it then categorizes planning uncertainty into structured target ambiguity and obstacle traversability, utilizing an LLM to resolve them in two stages. To eliminate target ambiguity, the agent grounds language descriptions to detected objects and iteratively refines the target candidates using tool calls and human queries. For obstacles, to minimize the expected interaction costs, we formulate hypothesis-augmented path planning and build a decision tree over traversability propositions. We then obtain an optimal querying policy via dynamic programming to efficiently guide two-way conversations until the definitive safe path is found. In the second mode, the robot performs real-time cooperative planning by maintaining a probabilistic belief over the human’s latent task intent, updated online from distance and motion-direction cues together with task completion status. Conditioned on this belief, the robot selects task-level actions using coordination-aware rules that prioritize cooperative tasks and avoid redundant effort on independent tasks. Together, the two planning modes enable a practical human-robot teammate that can both resolve decision-critical uncertainty and adapt online to evolving human intent/priorities in open-world collaboration.

For the experiments, we designed two tasks: human-

instructed planning under uncertain conditions and human-participated cooperation without communication to evaluate the two modules. The core planning engine is first evaluated in the Gazebo simulation, then integrated into the complete system along with a perception model, a voice control interface, and a low-level drone controller to be deployed in real-world scenarios. Compared with the baselines, the uncertainty-mitigation module significantly reduces the interaction cost by 51.9% while maintaining the 100% success rate. The intent-aware module achieves 74.3% average target prediction, thus saving the human-robot total travel distance and reducing the total task execution time by 25.4%.

The main contributions of this paper are as follows:

- We propose an uncertainty-mitigation joint planning module that efficiently resolves decision-critical uncertainty through human-robot bidirectional conversations. The module locates and handles both target ambiguity and traversability uncertainty. An optimal query strategy is then employed to minimize interaction costs to guide conversations for identifying a valid and reliable plan.
- We propose a real-time intent-aware collaboration module that maintains an online probabilistic belief over human intent and task progress, enabling the robot to adapt its cooperative strategy in real time without requiring explicit human feedback or retraining.
- We design and prototype a human-UAV collaborative planning system that integrates the two proposed planning modules with perception models and controllers. Experiments are conducted in both Gazebo simulators and open-world environments to verify its effectiveness.

II. CORE PLANNING ENGINE

The core planning engine, as the most critical component of the entire system, distinguishes this approach from other

solutions. It processes information provided by the perception model, resolves uncertainties within it, and ultimately generates high-level instructions as output. The uncertainties in the two planning modes are handled in distinct ways, which will be detailed separately in this chapter.

A. Uncertainty-Mitigation Joint Planning

We formulate the uncertainty-mitigation joint planning problem as follows. Consider an agent equipped with a perception module. At the onset of each task, a natural language instruction I is received, which may be ambiguous. The perception module then constructs a structured semantic map \mathcal{M} containing detected objects $O = \{o_1, o_2, \dots, o_n\}$, their positions, and extracted attributes such as color and obstacle probability. The expected output is a planned path consisting of a sequence of way-points.

In this task, uncertainty originates from semantic ambiguity in human commands, and perceptual uncertainty stems from partial observability. From the perspective of drafting a plan, these uncertainties mainly impact two factors: (1) *target selection* and (2) *object traversability*. Target uncertainty inevitably alters the entire plan, as the destination point varies. In contrast, the impact of the traversability of each object is conditional and can only be evaluated once a temporary target is established: several conflicting hypotheses regarding traversability paths can only be generated based on that for comparison. Therefore, the two factors should be analyzed separately and in a specific order. Note that, to reduce complexity, the uncertainty impact on obstacle-affected ranges is simply handled by introducing safety margins and is thus not considered explicitly.

To handle the uncertainties, we propose an uncertainty-mitigation joint planning module with human-robot two-way communication, as shown in Figure 1. First, the LLM drafts a plan prototype based on I , \mathcal{M} , and the current knowledge base \mathcal{K} . Each step is selected from an available action list. If the action is navigation, a target description in natural language will be added. Second, the agent grounds these natural language descriptions into the physical properties of detected objects within the operational field, utilizing both \mathcal{M} and \mathcal{K} . This process begins with the LLM assigning a prior probability to each object, indicating its likelihood of being the intended target. Thus, uncertainty in target selection occurs when the set of candidate objects $\mathcal{C}_{target} = \{o_i \in O \mid P_{LLM}(o_i = target | I, \mathcal{M}, \mathcal{K}) \geq \tau\}$ contains multiple elements, where the hyper-parameter τ is a threshold. In such cases, the agent utilizes available tools to acquire additional information, such as size/distance comparisons, random selection, or querying the human—and subsequently updates \mathcal{K} . This iterative process continues until a unique target is identified for each subtask.

Next, the agent addresses obstacle uncertainty by constructing a decision tree using the A* navigation algorithm with a hypothesis-augmented state space. When encountering an uncertain obstacle o_i with position v , the algorithm adds node $u = \langle v, H \cup \{o_i\} \rangle$ to the prioritized queue, where H is the current set of uncertain objects assumed to be passable,

starting from \emptyset . Each unique u will only be added once. If $\langle goal, H \rangle$ is reached for any H , then the corresponding path and H will be recorded as part of the output, and all nodes in the queue with H being a subset will be removed. Thus, the algorithm guarantees that paths with lower costs and stricter hypotheses always come first. After the algorithm is finished, a decision tree can thus be established in the order of path costs, with hypotheses being the branch conditions.

Finally, we formulate the problem as finding an optimal querying strategy with minimal total costs for querying and verification to determine the true path. Specifically, let n denote the total number of objects involved in hypotheses and impacting path-planning through the generated decision tree, each assigned a prior probability $p_i \in (0, 1)$ of being passable by the perception module. The generated decision tree inherently provides a deterministic mapping T from the 2^n possible environment configurations (the truth table) to m candidate paths. To resolve the remaining uncertainties, the agent actively queries humans with a subset of unknown objects U to get their traversability, incurring an interaction cost λ_1 and a verification cost λ_2 per object evaluated. Given that n is generally small, we compute an exact dynamic programming solution over the belief state space $s \in \{0, 1, unknown\}^n$. By recursively minimizing the Bellman equation:

$$V(s) = \min_U [\lambda_1 + |U|\lambda_2 + \mathbb{E}_{b(U)}[V(s \cup b(U))]], \quad (1)$$

$$V(s_0) = 0 \quad \text{for any } s_0 \text{ s.t. } |\{T(s_0)\}| = 1. \quad (2)$$

Here, $\{T(s_0)\}$ indicates the set of all possible paths matching belief s_0 , while $b(U)$ represents the binary beliefs about the traversability of U retrieved from human answers, with a prior possibility of $P(b(o_i)) = p_i$. The framework derives an optimal querying policy π , which guarantees that the robot identifies the definitive safe path with the absolute minimum expected interaction cost. The details about the search and querying are presented in Algorithm ??.

For the example shown in Figure 1, the user issues the instruction, "Pick up the medicine and deliver it to the injured person," which introduces semantic ambiguity by omitting the specific location of the medicine. In response, the agent constructs an initial probability distribution over detected objects and actively refines this target belief through queries via LLM. Once the target uncertainty is resolved, the system generates candidate paths and a corresponding decision tree conditioned on the traversability hypotheses of uncertain environmental elements (fire, net, and smoke). Notably, the traversability of the yellow box is implicitly pruned as it does not intersect any optimal path candidate. Finally, the agent executes the optimal querying strategy derived via dynamic programming, querying the operator regarding the fire and smoke while deferring questions about the net. This policy emerges because, despite the fire and the net equally impacting path selection, the fire's high prior probability of being an obstacle drastically reduces the expected necessity of subsequent queries regarding the net. Consequently, this sequential approach yields a lower expected total cost.

Algorithm 1: Uncertainty-Mitigation Joint Planning

Inputs: Start Position v_{start} , Goal v_{goal} , Uncertain object list O with priors $\{p_i\}_{i=1}^n$, Query cost λ_1 , Verification cost λ_2

Outputs: The definitive safe path P^*

```
1: Initialize priority queue  $Q \leftarrow \{\langle v_{start}, \emptyset \rangle\}$ ,  $\mathcal{P} \leftarrow \emptyset$ 
2: while  $Q$  is not empty and  $\langle v_{goal}, \emptyset \rangle$  is not reached do
3:   Pop  $u = \langle v, H \rangle$  from  $Q$  with the lowest path cost
4:   if  $v == v_{goal}$  then
5:     Add corresponding path and hypothesis  $H$  to  $\mathcal{P}$ 
6:     Remove all nodes  $\langle \cdot, H' \rangle$  from  $PQ$  where  $H \subseteq H'$ 
7:     continue
8:   for each valid neighbor  $v'$  of  $v$  do
9:      $H' \leftarrow H \cup \{v'\}$  if  $v' \in O_{unc}$  else  $H$ 
10:    Add unique node  $u' = \langle v', H' \rangle$  to  $PQ$ 
11: Extract the decision tree as a mapping  $T : \{0, 1\}^n \rightarrow \mathcal{P}$ 
    evaluating configurations against collected  $H$ 
12: Initialize memoization table  $V_{memo} \leftarrow \emptyset$ , Policy  $\pi^* \leftarrow \emptyset$ 
13: function MINCOST( $s$ )  $\triangleright s \in \{0, 1, \text{unknown}\}^n$ 
14:   if  $|\{T(s)\}| == 1$  then return 0
15:   if  $s \in V_{memo}$  then return  $V_{memo}[s]$ 
16:    $v_{min} \leftarrow \infty$ ,  $U^* \leftarrow \emptyset$ 
17:   for each subset  $U \subseteq \text{unknown}(s)$ ,  $U \neq \emptyset$  do
18:      $cost \leftarrow \lambda_1 + |U| \lambda_2 + \mathbb{E}_{b(U)|s}[\text{MINCOST}(s \cup b(U))]$ 
19:     if  $cost < v_{min}$  then
20:        $v_{min} \leftarrow cost$ ,  $U^* \leftarrow U$ 
21:    $V_{memo}[s] \leftarrow v_{min}$ ,  $\pi^*[s] \leftarrow U^*$ 
22:   return  $v_{min}$ 
23:  $s_0 \leftarrow (\text{unknown}, \dots, \text{unknown})$ 
24: COMPUTEMINCOST( $s_0$ )
25: Query human for  $\pi^*[s]$ , update belief  $s$ , until  $|\{T(s)\}| == 1$ 
26: return  $T(s)$ 
```

B. Real-time Intent-Aware Collaboration

We consider cooperative human–robot task execution in a shared workspace where a human-controlled agent and an autonomous robot operate concurrently to complete a finite set of perception-identified tasks. The human pursues an internal and unobserved objective, while the robot must adapt online using only the human’s recent motion and the evolving task completion status, without explicit communication.

Unlike conventional intent inference that emphasizes goal prediction alone, our setting involves multiple task types and therefore requires task type-aware coordination under uncertainty. Tasks may be independent (completable by any single agent) or cooperative (requiring simultaneous presence). A standard goal-following strategy directs the robot toward the most-likely human target. Such an assignment can be suboptimal: when the human selects an independent task, allocating the robot to the same task introduces redundant effort; when the task is cooperative, delayed convergence increases synchronization costs. These asymmetric coordination costs, together with noisy motion cues and real-time control constraints, motivate a lightweight intent belief coupled with a stability-aware coordination policy.

1) *Task model and state representation:* Let $\mathcal{T} = \mathcal{T}_{\text{ind}} \cup \mathcal{T}_{\text{coop}}$ denote the task set, where \mathcal{T}_{ind} are independent tasks and $\mathcal{T}_{\text{coop}}$ are cooperative tasks requiring both agents to participate. Each task t_i has a known location $x_i \in \mathbb{R}^2$.

At time t , the state is $s_t = (x_t^H, x_t^R, C_t)$, where x_t^H and x_t^R are the human and robot positions, and C_t is the set of completed tasks. The remaining tasks are $\mathcal{T}_t = \mathcal{T} \setminus C_t$. The robot observes x_t^H at each time and maintains C_t online.

2) *Lightweight intent belief update:* At each time step, the robot maintains a normalized belief over remaining tasks,

$$p_t(i) \triangleq P(g_t = t_i \mid x_{0:t}^H, C_t), \quad t_i \in \mathcal{T}_t, \quad (3)$$

where g_t denotes the human’s current task target. Completed tasks are masked by enforcing $p_t(i) = 0$ for $t_i \notin \mathcal{T}_t$ and renormalizing over \mathcal{T}_t .

We compute intent evidence from two local geometric cues: (1) distance-to-task and (2) heading alignment. For each candidate $t_i \in \mathcal{T}_t$, let $d_{t,i} = \|x_t^H - x_i\|_2$. Let the finite-difference velocity be $v_t = x_t^H - x_{t-1}^H$. When $\|v_t\|_2$ is below a threshold ε , we treat the heading cue as neutral; otherwise we compute alignment as the cosine between the human heading and the direction to the task, $c_{t,i} = \hat{v}_t^\top \hat{u}_{t,i}$, where $\hat{v}_t = v_t / \|v_t\|_2$ and $\hat{u}_{t,i} = (x_i - x_t^H) / \max(\|x_i - x_t^H\|_2, \varepsilon)$.

We convert these cues into a soft evidence score

$$\tilde{p}_t(i) = \exp(-\alpha d_{t,i} + \beta c_{t,i}), \quad (4)$$

with $\alpha > 0$ controlling distance sensitivity and $\beta \geq 0$ controlling directional influence. To accumulate evidence while remaining responsive, we apply exponential smoothing and then normalize:

$$p_t(i) \propto (1 - \gamma) p_{t-1}(i) + \gamma \tilde{p}_t(i), \quad \gamma \in (0, 1]. \quad (5)$$

This update is $O(|\mathcal{T}_t|)$ per step and runs at control rate.

3) *Coordination-aware task selection:* Given p_t , the robot selects a task-level target $a_t \in \mathcal{T}_t$ and executes motion via a low-level controller. Let $\hat{g}_t = \arg \max_{t_i \in \mathcal{T}_t} p_t(i)$ denote the most likely human target, with confidence $\rho_t = p_t(\hat{g}_t)$. The robot switches its target only when $\rho_t \geq \tau_{\text{intent}}$ and it is not already committed, where commitment is defined by being within a radius r_{commit} of the current target, as long as that target has not yet been completed. If $\rho_t < \tau_{\text{intent}}$, the robot maintains its current target; if no target is assigned, it selects the nearest remaining task. This prevents oscillatory switching under ambiguous intent estimates.

When switching is allowed, the action depends on the task type. If $\hat{g}_t \in \mathcal{T}_{\text{coop}}$, the robot sets $a_t = \hat{g}_t$ to reduce synchronization delay; if it arrives first, it waits up to a bounded timeout before re-evaluating the belief. If instead $\hat{g}_t \in \mathcal{T}_{\text{ind}}$, the robot selects complementary work by choosing the nearest remaining independent task other than \hat{g}_t (when available), thereby avoiding redundant effort; if no such task exists, it selects \hat{g}_t .

By coupling a lightweight geometric intent belief with task-type-aware role allocation and explicit stability gating, the robot adapts online to evolving human behavior, thereby minimizing redundant work, reducing cooperative waiting time, and maintaining stable real-time execution.



Fig. 2: Semantic Fusion: The top row displays the original RGB inputs. The bottom row illustrates the semantic segmentation masks after the recursive fusion strategy.

III. DETAILS OF SYSTEM DESIGN

To deploy and evaluate the proposed core planning engine in the real world, we established an end-to-end system connecting it with perception and low-level robot execution, which provides a central interface that acts as a voice assistant. By interpreting the operator’s voice instructions, it generates actionable scripts to carry out the entire task.

For environmental perception, a Vision-Language Model (VLM) first processes RGB-D sensor data to build a 3D semantic representation of the environment. This information is then presented in the central interface, providing real-time situational awareness for planning. Next, based on the task setting, one of the planning modules will be activated. Specifically, in uncertainty-mitigation joint planning, if the agent requires querying, it pauses execution and elicits a question in natural language, which is sent back to the voice module and converted to voice to ask the human operator for clarification. Once the uncertainty is completely removed, the modules generate a planned path in precise waypoints. In intent-aware collaboration, the system monitors the real-time positions of humans and the robot, analyzes human intent automatically, and then provides high-level control commands. These outputs are finally transmitted to the low-level drone controller, which is pre-trained with reinforcement learning following the method proposed in [31], to actuate the UAV and carry out the mission. The implementation of the perception and voice modules is as follows:

1) *VLM-Based 2D Perception*: A fundamental limitation of conventional perception systems is their reliance on fixed-label classifiers, which restrict adaptability in open-world navigation. To overcome this, our system employs the Grounded-SAM framework [32] to enable arbitrary natural language interaction, allowing the UAV to retrieve target objects by comparing prompt embeddings against stored 3D language-aligned descriptors. Specifically in this framework, Grounding DINO [33] detects objects and produces 2D bounding boxes, which are subsequently refined into high-quality segmentation masks using SAM [34].

2) *3D Semantic Map Representation*: We reconstruct the environment using 3D Gaussian Splatting [35], augmenting each anisotropic Gaussian with a semantic label ID, a confidence score $c \in [0, 1]$, and feature embeddings. This

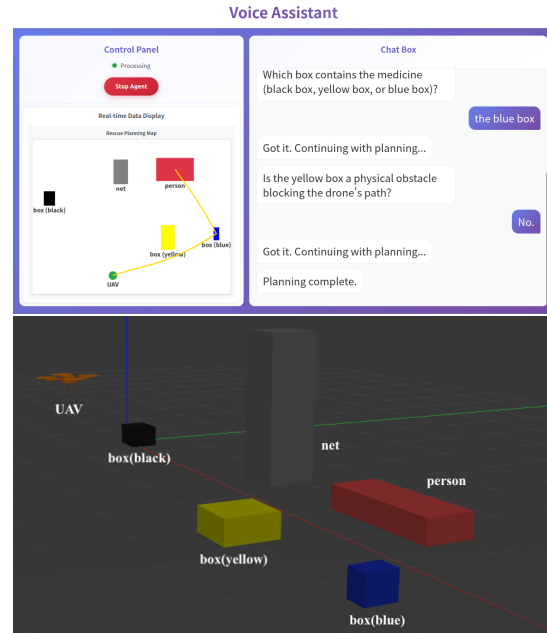


Fig. 3: Voice interface and Gazebo simulation environment.

representation supports efficient rasterization-based rendering, reprojecting the 3D semantic state onto the image plane to provide geometric and semantic references for incoming 2D observations. To ensure consistent data association, we implement a two-stage verification process. The system first evaluates cosine similarity between incoming 2D image features and latent 3D embeddings. Candidate matches are then validated against rendered semantic reprojections, providing a direct geometric reference. This hierarchical alignment fuses new observations into the correct spatial clusters, maintaining a stable 3D representation.

3) *Recursive Semantic Fusion*: Following association, a recursive fusion strategy maintains consistency across sequential frames. Although SAM provides high-quality masks, inaccurate boundaries in 2D segmentation models often corrupt 3D object geometry. We mitigate this by evaluating label consistency solely for pixels satisfying a strict depth continuity threshold ($\Delta z < 0.05\text{m}$). Matching labels trigger a confidence update via weighted averaging, whereas conflicts reduce the existing Gaussian confidence by a decay factor ($\gamma = 0.85$). To further harden the map against edge noise, confidence updates are weighted by a Euclidean distance transform of the 2D mask, prioritizing central pixels over noisy boundaries. This allows the 3D representation to self-correct over time, as shown in Fig. 2.

4) *Object Localization and Outlier Mitigation*: Segmented 3D object candidates are converted into axis-aligned bounding boxes in the navigation space. To remove sparse reconstruction outliers, we discard extreme points along each principal axis and retain the central 92% of the cluster when computing object bounds. Only candidates within the arena boundaries are retained for planning. By maintaining the DINO-based feature embeddings within the 3D map, our system supports natural language interaction. Users can provide a prompt, which is embedded into the same latent

space and compared against the stored 3D object features to retrieve the corresponding target object for planning.

5) *Voice Module*: The voice system implemented as a web application provides hands-free interaction for planning and control. We employ OpenAI Whisper for speech-to-text transcription, GPT-4o for dialogue understanding and command interpretation, and the OpenAI TTS API for speech synthesis. Integrating with the planning module, the system handles multi-turn communication and planning. The voice agent interface is shown in Figure 3.

IV. EXPERIMENTAL RESULTS

A. Simulation Verification

To evaluate the perception models exclusively, we first conduct simulation experiments in Gazebo, which is fully integrated with ROS2, as shown in Fig. 3.

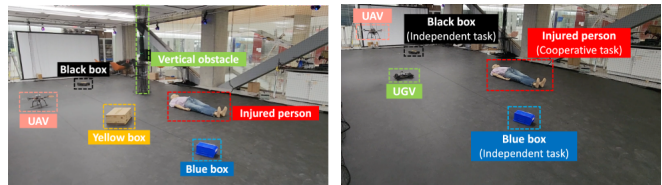
1) *Evaluation of the Uncertainty-Mitigation Joint Planning*: We compare the performance of the proposed uncertainty-mitigation module with two baselines: No querying and exhaustive querying. The first one directly plans the path without communication or uncertainty resolution, while the latter exhaustively queries humans for every uncertainty.

We design 20 simple scenarios with only one type of uncertainty and 5 complex scenarios with multiple sources of uncertainties in Gazebo to evaluate these methods. In each case, the uncertainty may arise from multiple target candidates or undetermined obstacles, and the agent requires additional information (target attributes like distance, size, color, or traversability of the obstacles) to provide the optimal plan. Each run is conducted 5 times to mitigate the randomness introduced by the LLM. We use ChatGPT-5.2 as the LLM backbone while removing its chain of thought feature and constraining the output to a structured format. We select the query cost $\lambda_1 = 10$ and verification cost $\lambda_2 = 1$.

The results are illustrated in Figure 6. The exhaustive baseline and the proposed method achieved a 100% success rate in both simple and complex scenarios, while the no-query baseline only achieved 71% in simple tasks and 40% in complex tasks due to a lack of information exchange with humans. A typical failure case is when the agent fails to identify the right target or makes false assumptions given a vague command. Even in successful cases, the no-query baseline always behaves conservatively to avoid any possible uncertainties, thus leading to a longer path being generated. On the other hand, the proposed method significantly reduces the query times by 56.8% and the total token usage by 30.3% with the adoption of hypothesis-based A* and dynamic programming to obtain the optimal query strategy.

2) *Evaluation of Real-Time Intent-Aware Collaboration*: We evaluate the intent-aware module in simulation against a non-cooperative baseline, where the robot selects the nearest uncompleted task as its target without modeling human intent or performing task-level coordination.

Four layouts are considered, each with two independent tasks and one cooperative task. Three are synthetic with distinct spatial configurations, and one is derived from the real-world setup with denser placement. For each layout,



(a) Planning Mode 1

(b) Planning Mode 2

Fig. 4: Evaluation setups: (a) shows the joint planning configuration, while (b) details the intent-aware setup.

both methods are tested under three human behavior cases, including two rational and one ambiguous pattern, across two human operators, yielding 24 runs per method.

The intent recognition parameters are fixed at $\alpha = 0.3$ and $\beta = 1.0$ with a confidence threshold of $\tau_{\text{intent}} = 0.5$. The commitment distance r_{commit} is set to 1.5 m for synthetic layouts and 1.0 m for the denser layout. If the robot reaches a cooperative task without the human, it waits up to 5 seconds before re-planning, and the human follows a similar short-wait strategy. Each episode terminates upon task completion. Results are reported as mean \pm standard error.

TABLE I: Simulation performance of the intent-aware cooperation module compared to the non-cooperative baseline.

Method	Time (s)	Total Dist (m)	Human Dist (m)
Proposed	14.83 \pm 0.79	24.46 \pm 1.41	12.26 \pm 0.76
Non-Cooperative	19.26 \pm 0.90	27.40 \pm 1.33	14.90 \pm 0.90

Table I summarizes overall simulation performance, where travel distance also serves as a proxy for motion-related energy cost. The proposed method reduces execution time by 23.0%, total travel distance by 10.7%, and human travel distance by 17.7% compared to the non-cooperative baseline. The substantial time reduction suggests fewer coordination delays and less redundant motion. The larger decrease in human distance further indicates that the drone assumes more of the workload and alleviates human effort.

TABLE II: Intent recognition performance measured by average true-target probability and top-1 accuracy.

Metric	Rational	Ambiguous	Overall
Avg. True-Target Prob.	75.2% \pm 2.2%	65.3% \pm 3.0%	71.9% \pm 2.0%
Top-1 Acc.	90.6% \pm 2.5%	70.7% \pm 3.2%	84.0% \pm 2.8%

Table II shows the intent recognition performance. The true target at each time step is approximated by the next task completed by the human. The overall true-target probability reaches 71.9%, well above the 33% uniform baseline. The corresponding top-1 accuracy is 84.0%, meaning that the highest-belief task matches the subsequently completed task in most cases. Performance is slightly lower in ambiguous scenarios, but the gap remains modest.

Figure 5 illustrates the temporal evolution of both methods. In the left panel, performance is similar early on, as the non-cooperative baseline completes nearby independent tasks efficiently. However, the proposed method advances faster

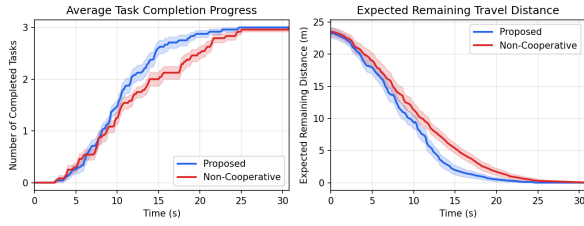


Fig. 5: Task completion progress (left) and expected remaining travel distance (right) over time for the proposed method and non-cooperative baseline.

during the cooperative phase and finishes earlier overall. The right panel shows the expected remaining travel distance based on shortest-path estimates; the steeper decline under the proposed method reflects more efficient coordination throughout execution.

B. Real-world Deployment

1) *Experimental Setup and Scene Composition:* As shown in Fig. 4, experiments were conducted in a $12\text{m} \times 6\text{m}$ motion-captured indoor space configured for two distinct evaluation scenarios. For the human-robot joint planning scenario, the scene included five entities: a human mannequin (injured person), a black box, and a blue box acting as potential task targets, alongside a yellow box and a vertical net serving as static obstacles. Conversely, for the human intent aware planning scenario, the environment featured two independent tasks (the black and blue boxes) and one cooperative task (the injured person) shared between the autonomous UAV and a human-teleoperated UGV. Both high-level planning modules operated at a frequency of 100 Hz to ensure real-time coordination.

To construct the semantic map, RGB-D images were acquired using an ORBBEC Gemini 336L camera, while a Vicon motion-capture system provided ground-truth camera poses at 200 Hz. This setup enabled the real-time fusion of observations into a consistent global 3D frame. The resulting refined 2D bounding box coordinates and their corresponding Grounding DINO confidence scores for the objects are summarized in Table III.

TABLE III: 2D Object Localizations and Confidence Scores.

Attribute	Blue box	Black box	People	Yellow Box	Net
Confidence	0.8147	0.6342	0.5336	0.4644	0.3371
Range x	[7.39, 7.64]	[-0.02, 0.47]	[4.89, 6.53]	[5.10, 5.70]	[3.02, 3.66]
Range y	[-1.04, -0.68]	[-0.09, 0.30]	[0.58, 1.21]	[-1.30, -0.62]	[0.49, 1.17]

To physically execute these planned behaviors, a custom quadrotor platform was developed, equipped with an onboard NVIDIA Jetson TX2 flight computer and an IMU sensor. The core flight software and Extended Kalman Filter (EKF) for state estimation were implemented in C++, communicating via ROS2 with the PyTorch-based RL models implemented in Python. Operating at 200Hz, this dedicated low-level RL controller seamlessly tracked and actuated the desired waypoints generated by the high-level planning modules.

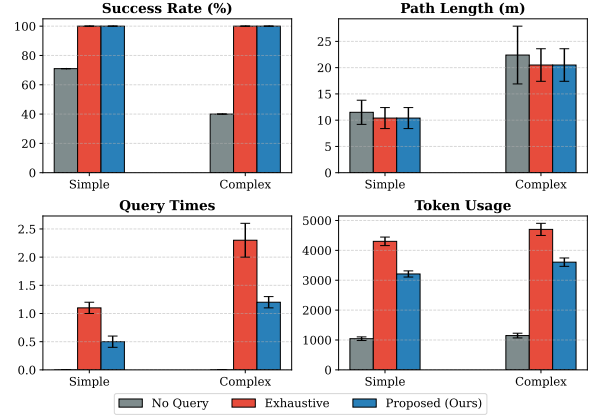


Fig. 6: Visualized results of uncertainty-mitigation in Gazebo simulations. Note that we only compare paths successfully generated by all three methods for length comparison.

2) *Evaluation of Uncertainty-mitigation Joint Planning:* We first evaluate the joint planning model using the same search-and-rescue scenario as in the simulation. We run three times with identical object locations, while a different command is given in each task (“Get the medicine from the box and deliver it to the person.”; “Pick up the medicine from the box, deliver it to the person and back to your initial position.”; “Pick up medicine from the black box and then take the bandage from the blue box and deliver both of them to the person”). All communications are done by voice. The planning process will run for 5 times to mitigate the randomness, while one of the them will be deployed to record the success rate. The results are shown in Table V.

In the first two commands, the box is not specified; thus, the passive baseline always drives the UAV to the yellow box, which is nearest to the UAV but is supposed to be an obstacle, causing a significantly low success rate. On the other hand, the other two methods always ask a human first to find out the true box containing the medicine. However, as both the yellow box and the vertical obstacle are considered potential obstacles for the UAV, our proposed method only asks the human when any of the obstacles impact the planning, while the exhaustive baseline always verifies the two objects first and then starts to plan. As a result, our method reaches 100% success rate while reducing the number of queries by 51.9% and 16.4% of the total tokens used.

3) *Evaluation of Intent-Aware Cooperation:* We evaluate the intent-aware cooperation module on the physical system using the same two methods and human behavior cases as in simulation, with identical intent inference parameters.

Table IV summarizes the results. Compared to the non-cooperative baseline, the proposed method reduces execution time by 25.4%, total travel distance by 17.9%, and human travel distance by 18.3%. Execution time is naturally longer than in simulation due to physical dynamics, actuation limits, and sensing noise. Nevertheless, the relative performance improvement remains consistent, indicating effective transfer from simulation to real-world deployment.

For intent recognition, the average true-target probability

reaches 74.3%, and the top-1 accuracy reaches 95.0%, both well above a uniform baseline. The high top-1 accuracy indicates that the inferred belief most often assigns the highest probability to the task subsequently completed by the human. Despite real-world disturbances, the belief remains aligned with observed human actions, suggesting stable intent estimation under physical execution constraints.

TABLE IV: Real-world performance of the intent-aware co-operation module compared to the non-cooperative baseline.

Method	Time (s)	Total Dist (m)	Human Dist (m)
Proposed	20.59 ± 1.25	16.31 ± 1.91	9.22 ± 2.66
Non-Cooperative	27.61 ± 2.99	19.86 ± 2.88	11.29 ± 2.38

TABLE V: Real-world experimental results for uncertainty-mitigation joint planning, averaged on three commands.

Method	Success (%)	Queries	Tokens	Time (s)
Passive	33.3	0.0	1079.3 ± 50.2	8.80 ± 1.07
Exhaustive	100	2.7	4109.0 ± 81.1	13.35 ± 1.51
Ours	100	1.3	3434.8 ± 74.2	11.84 ± 1.47

V. CONCLUSION

In this paper, we propose an end-to-end, unified human-robot joint planning system designed to effectively address dual sources of uncertainty in open-world collaboration. By operating in two complementary modes, our system enables autonomous agents to act as proactive, human-like teammates rather than passive tools. Within the core planning engine of the system, the uncertainty-mitigation joint planning module resolves uncertainties through an LLM-guided active elicitation mechanism with strictly minimized interaction costs. Additionally, the real-time intent-aware collaboration module infers the human’s latent objectives using uncommunicated spatial and directional cues, continuously updating a probabilistic belief to enable adaptive task coordination. Extensive evaluations in both Gazebo simulations and real-world UAV deployments show that our system significantly outperforms conventional baselines in both modes, reducing the required interaction cost by 51.9% and accelerating the total cooperative task execution time by 25.4%.

Future work will focus on tightly coupling these two modes, allowing the robot to dynamically transition from implicit intent inference to explicit querying when behavioral confidence drops, and scaling the framework to multi-agent, multi-human scenarios under complex temporal constraints.

ACKNOWLEDGMENT

The authors acknowledge Maneesha Wickramasuriya, Mason Husling, and Jaden Shin from the Department of Mechanical and Aerospace Engineering at the George Washington University for their assistance with the hardware development and real-world verification experiments[36], [37], [38], [39], [40], [41].

REFERENCES

- [1] R. Zhang, N. J. McNeese, G. Freeman, and G. Musick, “an ideal human” expectations of ai teammates in human-ai teaming,” *Proceedings of the ACM on Human-Computer Interaction*, vol. 4, no. CSCW3, pp. 1–25, 2021.
- [2] A. I. Hauptman, B. G. Schelble, N. J. McNeese, and K. C. Madathil, “Adapt and overcome: Perceptions of adaptive autonomous agents for human-ai teaming,” *Computers in Human Behavior*, vol. 138, p. 107451, 2023.
- [3] S. Berretta, A. Tausch, G. Ontrup, B. Gilles, C. Peifer, and A. Kluge, “Defining human-ai teaming the human-centered way: a scoping review and network analysis,” *Frontiers in Artificial Intelligence*, vol. 6, p. 1250725, 2023.
- [4] W. Xu and Z. Gao, “Applying hcai in developing effective human-ai teaming: A perspective from human-ai joint cognitive systems,” *interactions*, vol. 31, no. 1, pp. 32–37, 2024.
- [5] Z. Fang, J. Zhao, M. Yang, Z. Lu, W. Zhou, and H. Li, “Coordinate-aligned multi-camera collaboration for active multi-object tracking,” *Multimedia Systems*, vol. 30, no. 4, p. 221, 2024.
- [6] O. Lockwood and M. Si, “A review of uncertainty for deep reinforcement learning,” in *Proceedings of the AAAI Conference on Artificial Intelligence and Interactive Digital Entertainment*, vol. 18, pp. 155–162, 2022.
- [7] L. Zhao, W. McClinton, A. Curtis, N. Kumar, T. Silver, L. P. Kaelbling, and L. L. Wong, “Seeing is believing: Belief-space planning with foundation models as uncertainty estimators,” *arXiv preprint arXiv:2504.03245*, 2025.
- [8] M. Aghzal, E. Plaku, G. J. Stein, and Z. Yao, “A survey on large language models for automated planning,” *arXiv preprint arXiv:2502.12435*, 2025.
- [9] S. Ambhore, “A comprehensive study on robot learning from demonstration,” in *2020 2nd International Conference on Innovative Mechanisms for Industry Applications (ICIMIA)*, pp. 291–299, IEEE, 2020.
- [10] A. Obaigbena, O. A. Lottu, E. D. Ugwuanyi, B. S. Jacks, E. O. Sodiya, O. D. Daraojimba, et al., “Ai and human-robot interaction: A review of recent advances and challenges,” *GSC Advanced Research and Reviews*, vol. 18, no. 2, pp. 321–330, 2024.
- [11] Y. Li, S. Tang, R. Chen, F. X. Yu, G. Jiang, M. Imani, N. D. Bastian, and T. Lan, “Aczero: Graph-embedding-based tree search for mastering automated cyber defense,” *arXiv preprint arXiv:2601.02196*, 2026.
- [12] T. Mandel, Y.-E. Liu, E. Brunskill, and Z. Popović, “Where to add actions in human-in-the-loop reinforcement learning,” vol. 31, 2017.
- [13] E. Mosqueira-Rey, E. Hernández-Pereira, D. Alonso-Ríos, J. Bobes-Bascarán, and Á. Fernández-Leal, “Human-in-the-loop machine learning: a state of the art,” *Artificial Intelligence Review*, vol. 56, no. 4, pp. 3005–3054, 2023.
- [14] S. Lemaignan, M. Warnier, E. A. Sisbot, A. Clodic, and R. Alami, “Artificial cognition for social human-robot interaction: An implementation,” *Artificial Intelligence*, vol. 247, pp. 45–69, 2017.
- [15] S. Teso and K. Kersting, “Explanatory interactive machine learning,” in *Proceedings of the 2019 AAAI/ACM Conference on AI, Ethics, and Society*, pp. 239–245, 2019.
- [16] W. Huang, P. Abbeel, D. Pathak, and I. Mordatch, “Language models as zero-shot planners: Extracting actionable knowledge for embodied agents,” in *International conference on machine learning*, pp. 9118–9147, PMLR, 2022.
- [17] M. Awais and D. Henrich, “Proactive premature intention estimation for intuitive human-robot collaboration,” in *2012 IEEE/RSJ International Conference on Intelligent Robots and Systems*, pp. 4098–4103, IEEE, 2012.
- [18] M. Dhanda, B. A. Rogers, S. Hall, E. Dekoninck, and V. Dhokia, “Reviewing human-robot collaboration in manufacturing: Opportunities and challenges in the context of industry 5.0,” *Robotics and Computer-Integrated Manufacturing*, vol. 93, p. 102937, 2025.
- [19] Z. Fang, T. Lan, and M. Imani, “Mint: Minimal information neuro-symbolic tree for objective-driven knowledge-gap reasoning and active elicitation,” *arXiv preprint arXiv:2602.05048*, 2026.
- [20] D. Ghose, O. Gitelson, R. Jin, G. Abawe, M. Vázquez, and B. Scasellati, “I’ve changed my mind: Robots adapting to changing human goals during collaboration,” *IEEE Robotics and Automation Letters*, vol. 11, no. 2, pp. 1490–1497, 2025.
- [21] K. Inkpen, S. Chappidi, K. Mallari, B. Nushi, D. Ramesh, P. Michelucci, V. Mandava, L. H. Vepřek, and G. Quinn, “Advancing human-ai complementarity: The impact of user expertise and

- algorithmic tuning on joint decision making,” *ACM Transactions on Computer-Human Interaction*, vol. 30, no. 5, pp. 1–29, 2023.
- [22] H. Ali, P. Allgeuer, and S. Wermtter, “Comparing apples to oranges: Llm-powered multimodal intention prediction in an object categorization task,” in *International conference on social robotics*, pp. 292–306, Springer, 2024.
- [23] G. Hoffman, T. Bhattacharjee, and S. Nikolaidis, “Inferring human intent and predicting human action in human–robot collaboration,” *Annual Review of Control, Robotics, and Autonomous Systems*, vol. 7, no. 1, pp. 73–95, 2024.
- [24] M. Alali and M. Imani, “Deep reinforcement learning data collection for bayesian inference of hidden markov models,” *IEEE transactions on artificial intelligence*, vol. 6, no. 5, pp. 1217–1232, 2024.
- [25] S. Ni, L. Zhao, A. Li, D. Wu, and L. Zhou, “Cross-view human intention recognition for human-robot collaboration,” *IEEE Wireless Communications*, vol. 30, no. 3, pp. 189–195, 2023.
- [26] D. Hadfield-Menell, S. J. Russell, P. Abbeel, and A. Dragan, “Cooperative inverse reinforcement learning,” *Advances in neural information processing systems*, vol. 29, 2016.
- [27] T. Mai, T. Nguyen, *et al.*, “Inverse factorized soft q-learning for cooperative multi-agent imitation learning,” *Advances in Neural Information Processing Systems*, vol. 37, pp. 27178–27206, 2024.
- [28] Z. Fang, J. Zhao, W. Zhou, and H. Li, “Implementing first-person shooter game ai in wild-scav with rule-enhanced deep reinforcement learning,” in *2023 IEEE Conference on Games (CoG)*, pp. 1–8, IEEE, 2023.
- [29] S. Tang, J. Chen, and T. Lan, “Malinzero: Efficient low-dimensional search for mastering complex multi-agent planning,” in *The Thirty-ninth Annual Conference on Neural Information Processing Systems*.
- [30] H. Liu, Y. Tong, G. Liu, Z. Ju, and Z. Zhang, “Idagc: Adaptive generalized human-robot collaboration via human intent estimation and multimodal policy learning,” in *2025 IEEE/RSJ International Conference on Intelligent Robots and Systems (IROS)*, pp. 4480–4487, IEEE, 2025.
- [31] B. Yu and T. Lee, “Equivariant reinforcement learning frameworks for quadrotor low-level control,” *IEEE Transactions on Control Systems Technology*, vol. 34, no. 1, pp. 86–99, 2026.
- [32] T. Ren, S. Liu, A. Zeng, J. Lin, K. Li, H. Cao, J. Chen, X. Huang, Y. Chen, F. Yan, *et al.*, “Grounded sam: Assembling open-world models for diverse visual tasks,” *arXiv preprint arXiv:2401.14159*, 2024.
- [33] S. Liu, Z. Zeng, T. Ren, F. Li, H. Zhang, J. Yang, Q. Jiang, C. Li, J. Yang, H. Su, *et al.*, “Grounding dino: Marrying dino with grounded pre-training for open-set object detection,” in *European conference on computer vision*, pp. 38–55, Springer, 2024.
- [34] A. Kirillov, E. Mintun, N. Ravi, H. Mao, C. Rolland, L. Gustafson, T. Xiao, S. Whitehead, A. C. Berg, W.-Y. Lo, *et al.*, “Segment anything,” in *Proceedings of the IEEE/CVF international conference on computer vision*, pp. 4015–4026, 2023.
- [35] B. Kerbl, G. Kopanas, T. Leimkühler, G. Drettakis, *et al.*, “3d gaussian splatting for real-time radiance field rendering,” *ACM Trans. Graph.*, vol. 42, no. 4, pp. 139–1, 2023.
- [36] R. Chen, J. Kwon, W.-H. Chen, and C. Sung, “Design and characterization of a pneumatic tunable-stiffness bellows actuator,” in *2024 IEEE 7th International Conference on Soft Robotics (RoboSoft)*, pp. 997–1003, IEEE, 2024.
- [37] R. Chen, J. Kwon, K. Wu, and W.-H. Chen, “Tunable leg stiffness in a monopodal hopper for energy-efficient vertical hopping across varying ground profiles,” in *2025 IEEE International Conference on Robotics and Automation (ICRA)*, pp. 12929–12935, IEEE, 2025.
- [38] S. Misra, M. Mitchell, R. Chen, and C. Sung, “Design and control of a tunable-stiffness coiled-spring actuator,” in *2023 IEEE International Conference on Robotics and Automation (ICRA)*, no. 72, 2023.
- [39] B. Liao, Z. Zhao, L. Chen, H. Li, D. Cremers, and P. Liu, “Global-pointer: Large-scale plane adjustment with bi-convex relaxation,” in *European Conference on Computer Vision*, pp. 360–376, Springer, 2024.
- [40] B. Liao, Z. Zhao, H. Li, Y. Zhou, Y. Zeng, H. Li, and P. Liu, “Convex relaxation for robust vanishing point estimation in manhattan world,” in *Proceedings of the Computer Vision and Pattern Recognition Conference*, pp. 15823–15832, 2025.
- [41] S. Yan, P. Shi, Z. Zhao, K. Wang, K. Cao, J. Wu, and J. Li, “Turboreg: Turboclique for robust and efficient point cloud registration,” in *Proceedings of the IEEE/CVF International Conference on Computer Vision*, pp. 26371–26381, 2025.